Biochemical Journal (2019) **476** 1433–1444
https://doi.org/10.1042/BCJ20190138

Research Article

Multi-functional regulator MapZ controls both positioning and timing of FtsZ polymerization

Zhang Feng, Jiahai Zhang, Da Xu, Yong-Liang Jiang, Cong-Zhao Zhou and Yuxing Chen

School of Life Sciences and Hefei National Laboratory for Physical Sciences at the Microscale, University of Science and Technology of China, Hefei, Anhui 230027, People's Republic of China

Correspondence: Yuxing Chen (cyxing@ustc.edu.cn)

The tubulin-like GTPase protein FtsZ, which forms a discontinuous cytokinetic ring at mid-cell, is a central player to recruit the division machinery to orchestrate cell division. To guarantee the production of two identical daughter cells, the assembly of FtsZ, namely Z-ring, and its precise positioning should be finely regulated. In *Streptococcus pneumoniae*, the positioning of Z-ring at the division site is mediated by a bitopic membrane protein MapZ (mid-cell-anchored protein Z) through direct interactions between the intracellular domain (termed MapZ-N (the intracellular domain of MapZ)) and FtsZ. Using nuclear magnetic resonance titration experiments, we clearly assigned the key residues involved in the interactions. In the presence of MapZ-N, FtsZ gains a shortened activation delay, a lower critical concentration for polymerization and a higher cooperativity towards GTP hydrolysis. On the other hand, MapZ-N antagonizes the lateral interactions of single-stranded filaments of FtsZ, thus slows down the formation of highly bundled FtsZ polymers and eventually maintains FtsZ at a dynamic state. Altogether, we conclude that MapZ is not only an accelerator to trigger the polymerization of FtsZ, but also a brake to tune the velocity to form the end-product, FtsZ bundles. These findings suggest that MapZ is a multi-functional regulator towards FtsZ that controls both the precise positioning and proper timing of FtsZ polymerization.

Introduction

FtsZ, namely filamentous temperature-sensitive Z, is an ancient tubulin-like GTPase that initiates bacterial cell division via forming a ring-like structure (known as the Z-ring) at the septum. In the cell division process, individual FtsZ molecules polymerize into protofilaments, which are subsequently integrated into a proto ring at the site of cytokinesis [1–3]. This proto ring further serves as a scaffold to recruit a large number of downstream division proteins and eventually constitutes the divisome [4–6]. The constriction of the Z-ring accompanying with the synthesis and splitting of septal peptidoglycan enables the divisome to divide the mother cell into identical daughter cells [7,8].

The Z-ring is a dynamic structure, and the exchange of FtsZ monomers [9] requires the energy input via the hydrolysis of guanosine-5'-triphosphate (GTP) [10]. It has long been recognized that FtsZ polymerized into a closed ring-like structure around the cell periphery [11,12]. However, the recent high-resolution imaging and Cryo-electron tomography observed a discontinuous structure of loosely bundled FtsZ filaments [13–17]. Extensive studies suggested that FtsZ cooperatively formed polymers of different lengths and structures, such as single-stranded filaments, bundles, tubules and sheets, depending on the experimental conditions [18–24]. To guarantee the production of two identical daughter cells, the assembly and positioning of the Z-ring need to be strictly regulated [25–27]. Moreover, the lateral interactions between FtsZ filaments that contribute to the formation of various high-order structures are also important to the architecture and function of the Z-ring. In addition,

Received: 26 February 2019
Revised: 25 April 2019
Accepted: 26 April 2019

Accepted Manuscript online: 29 April 2019
Version of Record published: 21 May 2019

Biochemical Journal (2019) **476** 1433–1444
https://doi.org/10.1042/BCJ20190138

the positively charged C-terminal tail of FtsZ was reported to facilitate lateral interactions via shielding negatively charged filaments [28,29]. However, the fine mechanism that regulates the Z-ring dynamics remains unclear due to the complexity of Z-ring formation.

Biochemical and biophysical analyses suggest that *Streptococcus pneumoniae* FtsZ exhibits a delay of GTPase activity but not of filament polymerization, indicating the FtsZ polymer should undergo a transition from the inactive to active state of GTPase [30]. Moreover, the positioning of *S. pneumoniae* Z-ring at the division site was achieved by a bitopic membrane protein, MapZ (mid-cell-anchored protein Z) (also termed LocZ), which functions as a molecular beacon signaling the position of the future division site [31,32]. In contrast with this positive positioning of FtsZ, rod-shaped bacteria usually adopt a negative regulatory mechanism, such as the nucleoid occlusion system and the Min system [33,34]. Further study showed that MapZ is crucial for the correction of the angle of Z-ring towards the cell length axis [35]. The solution structures revealed a bi-module structure of the extracellular domain of MapZ, the C-terminal subdomain of which is projected outwards to bind to the nascent peptidoglycan [36].

Based on biochemical and biophysical studies, here we revealed a new function of MapZ that serves as a regulator for FtsZ assembly. We found that MapZ functions as a double-edged sword to facilitate the formation of FtsZ single-stranded filaments and attenuate the bundling of FtsZ. These findings provided novel insights into the fine spatial and temporal regulation of MapZ towards FtsZ.

Materials and methods

Cloning and expression of FtsZ, MapZ-N and MapZ-N_{mut}

The coding regions of FtsZ and MapZ were amplified from the genomic DNA of *S. pneumoniae* R6. The full-length FtsZ was cloned into a pET28a-derived expression vector without His-tag and the intracellular domain of MapZ covering residues from Met1 to Lys158, termed MapZ-N (the intracellular domain of MapZ), was cloned into a 2B-T vector with an N-terminal hexa-histidine tag using ligation-independent cloning system. The *E. coli* BL21 (DE3) strain was used for the expression of recombinant proteins. The transformed cells were grown at 37°C in LB culture medium (10 g NaCl, 10 g Bacto-Tryptone and 5 g yeast extract per liter) containing appropriate antibiotics until the OD_{600nm} reached 0.6. Protein expression was then induced with 0.2 mM isopropyl β-D-1-thiogalactopyranoside (IPTG) for another 4 h at 37°C and cells were harvested by centrifugation at 6000×***g*** for 10 min at 4°C. The harvested cells were resuspended in PEM buffer (50 mM PIPES, pH 6.5, 5 mM $MgCl_2$, 1 mM EDTA) and TNG buffer (20 mM Tris–HCl, pH 7.5, 100 mM NaCl, 5% glycerol) for FtsZ and MapZ-N, respectively. The nine-residue mutant MapZ-N_{mut} (the 9-residue mutant of MapZ-N) was obtained using the MutExpress™ Fast Mutagenesis Kit with the plasmid encoding the wild-type MapZ-N as the template. The mutant protein was expressed in the same manner as the wild-type protein.

Purification of FtsZ, MapZ-N and MapZ-N_{mut}

To purify FtsZ proteins, the *E. coli* cells were lysed by sonication, and the soluble fraction containing FtsZ was purified by Ca^{2+}-induced precipitation. Briefly, after 12 min of sonication and centrifugation at 100 000×***g*** for 30 min at 4°C, the supernatant containing the soluble target protein was collected. Then GTP and $CaCl_2$ were added to the supernatant at the final concentration of 1 and 20 mM, respectively. The sample was incubated for 15 min at 30°C and then centrifuged at 12 000×***g*** for 15 min at 4°C. The pellet containing FtsZ was resuspended in 20 ml PEM buffer and centrifuged as in the previous step to discard the insoluble fraction. The supernatant was subjected to another cycle of Ca^{2+}-induced precipitation. The final FtsZ pellet was resuspended in 5 ml TEM buffer (50 mM Tris–HCl, pH 8.0, 0.1 mM EDTA, 5 mM $MgCl_2$) and further purified by anion exchange chromatography using a 5 ml HiTrap QHP column (GE Healthcare) equilibrated in the same buffer. The column was washed with the equilibration buffer and the protein was eluted with a gradient KCl from 0 to 1 M. The target protein was eluted in a range of 300–400 mM KCl and were further pooled and desalted against TKM buffer (20 mM Tris–HCl, pH 7.5, 250 mM KCl, 5 mM $MgCl_2$). The protein purity was evaluated by electrophoresis and samples were stored at −80°C.

To purify MapZ-N and MapZ-N_{mut} protein, the *E. coli* cells were lysed by 12 min sonication and centrifuged at 12 000×***g*** for 30 min. The supernatant containing the soluble target protein was collected and loaded onto a Ni-NTA column (Qiagen, Mississauga ON) equilibrated with the TNG buffer (20 mM Tris–HCl, pH 7.5, 100 mM NaCl, 5% glycerol). The target protein was eluted with 400 mM imidazole and further purified by anion exchange chromatography as described above. The elution sample was then loaded to Superdex 75

column (GE Healthcare) equilibrated in TNG buffer. The peak containing the target protein samples were pooled and protein purity was evaluated by electrophoresis and samples were stored at −80°C.

All protein samples needed for biochemical experiments were freshly prepared and samples for enzymatic activity assays were collected at the highest peak fractions without concentration and stored at −80°C with 30% glycerol.

GTPase activity assays

The GTPase activity of FtsZ was assayed in the buffer containing 20 mM HEPES pH 6.5, 250 mM KCl, 5 mM $MgCl_2$ and 1 mM GTP (Sigma) with or without the addition of MapZ-N. The reaction in a total volume of 20 μl was triggered by adding the purified FtsZ of different final concentrations, followed by incubation at 37°C for different time courses and finally stopped by heating at 95°C for 10 min. After centrifugation at 12 000×**g** for 10 min, the supernatant was applied to HPLC (Agilent 1200 Series, U.S.A.) analyses. The buffer of 100 mM KH_2PO_4/K_2HPO_4, pH 6.5, 10 mM tetrabutyl ammonium bromide was used for equilibration of the column (Zorbax 300SB-C18 column, 4.6 × 150 mm, Agilent, U.S.A.) and separation of the components at a flow rate of 1 ml/min. The production of GDP was monitored via the absorption at 254 nm. The kinetic determinations of FtsZ were performed at different GTP concentrations, and the K_m and V_{max} values were calculated by non-linear fitting to the Michaelis–Menten equation using the program Origin 8. The Hill coefficient was calculated by the Hill equation. Three independent assays were performed to calculate the means and standard deviations.

90° light scattering assays

The 90° light scattering experiments were performed following a previous report [37]. In general, light scattering was measured in a Hitachi F-2700 fluorescence spectrophotometer using a quartz cuvette that was maintained at 30°C by a circulating water bath. Both excitation and emission wavelengths were set at 350 nm with a slit width of 5 nm in all assays. For the standard polymerization assay, MapZ-N and/or FtsZ were incubated in the cuvette at 30°C in polymerization buffer in a total volume of 0.15 ml. After establishing a baseline for 2 min, polymerization was induced by the addition of 1 mM GTP to the reaction mixture. The sample was gently mixed with a pipet tip, and light scattering was monitored for an additional 22 min. Data were collected with an interval of 2 s, and light scattering following GTP addition was plotted as a function of time.

Electron microscopy analyses

To evaluate the effect of MapZ-N on FtsZ bundling, the FtsZ polymer morphology was visualized using negative-staining transmission electron microscopy (EM). The polymerization reactions with 15 μM FtsZ (with and without MapZ-N) were triggered upon addition of 1 mM GTP. Followed by incubation at the room temperature for 3 min, the samples were adsorbed to carbon-coated glow-discharged grids for 1 min. After blotting excess liquid off, the sample was immediately stained for 1 min with 1% (wt/vol) uranyl acetate and blotted off. Grids were examined with an FEI Technai G2 120 KV transmission electron microscope.

Microscale thermophoresis assays

Microscale thermophoresis (MST) analyses were carried out with a Monolith NT.115 instrument (Nano Temper, Munich, Germany). Purified FtsZ was covalently linked to the fluorescent label NT-495 by NHS coupling. Increasing concentrations of unlabeled MapZ-N (12 nM to 0.4 mM) or MapZ-N_{mut} (12 nM to 0.4 mM) in 20 mM HEPES pH 6.5, 250 mM KCl, 5 mM $MgCl_2$, 0.05% Tween-20 were titrated against constant amounts of labeled FtsZ (0.2 μM). Standard treated capillaries (K002 Monolith NT.115) were loaded with the samples. Experiments were carried out in standard treated capillaries with 20% LED power and 80% IR-laser at 25°C. Data were treated with NT analysis software (NanoTemper) to determine dissociation constants (K_d).

NMR spectroscopy, data processing

Both ^{15}N-labeled and $^{15}N/^{13}C$-labeled MapZ-N samples were dissolved to a final concentration of 0.6 mM in 500 μl buffer containing 50 mM phosphate sodium, pH 6.5, 100 mM NaCl in a 90% H_2O and 10% D_2O mixture or in 99.96% D_2O. All NMR experiments were carried out at 298 K on Bruker Avance600 spectrometer equipped with the cryoprobe. The following spectra were recorded to obtain the backbone and side chain resonance assignments: 2D $^1H–^{15}N$ heteronuclear single quantum coherence (HSQC) and 3D HNCO, HN(CA)

Biochemical Journal (2019) 476 1433–1444
https://doi.org/10.1042/BCJ20190138

CO, CBCA(CO)-NH, CBCANH, (H)C(CO)NH-TOCSY, HBHA(CBCA)-(CO)NH, H(C)(CO)NH-TOCSY, HCCH-COSY and HCCH-TOCSY. NMR data were then processed using NMRPipe and analyzed with Sparky3 and Cyana3.97.

For titration experiments, unlabeled FtsZ proteins were prepared with a final concentration of 0.4 mM and the buffer contains 50 mM phosphate sodium, pH 6.5, 50 mM NaCl. NMR titration experiments were performed by adding increasing amounts of unlabeled FtsZ to uniformly ^{15}N-labeled MapZ-N. A series of ^{1}H–^{15}N HSQC spectra were recorded at FtsZ/MapZ-N mole ratios of 0.25 : 1, 0.5 : 1, 0.75 : 1 and 1 : 1.25. The ^{1}H and ^{15}N resonance variations were applied to collecting HSQC experiments at 298 K. Combined chemical shift perturbation was calculated using the following equation,

$$\Delta = \sqrt{\Delta_{^{1}\mathrm{H}}^{2} + (0.17\Delta_{^{15}\mathrm{N}})^{2}}$$

where $\Delta_{^{1}\mathrm{H}}$ and $\Delta_{^{15}\mathrm{N}}$ are chemical shift changes in the ^{1}H and ^{15}N dimensions, respectively.

Results

Mapping the key residues of MapZ-N interacting with FtsZ

MapZ is a bitopic membrane protein, the C-terminal extracellular domain (MapZ-C) of which binds to the peptidoglycan whereas the N-terminal intracellular domain (MapZ-N) positions FtsZ at the division site via direct protein–protein interaction [36]. As shown in Figure 1A, the profile indicated that the input mixture of MapZ-N and FtsZ at a molar ratio of 1 : 1 gave a single peak of ~71 kDa, which is identical with the sum of the theoretical molecular mass of individual MapZ-N and FtsZ. Subsequent gel electrophoresis analyses confirmed that the fractions contain both MapZ-N and FtsZ, which share a similar molarity as estimated from the intensity of the stained bands (Figure 1B). To further determine the dissociation constant (K_d) of the two proteins, we applied MST experiments and revealed a K_d of 0.53 ± 0.18 μM for MapZ-N towards FtsZ (Figure 1C). Together, these results enabled us to confirm that MapZ-N and FtsZ form a stable complex with a stoichiometry of 1 : 1.

Despite the previous report suggested the N-terminal segment of 40 residues is critical for MapZ binding to FtsZ [31], the precise interface on MapZ-N remains unknown. We titrated FtsZ protein into MapZ-N solution using NMR experiments and monitored the chemical shifts of backbone atoms. A series of ^{1}H–^{15}N HSQC spectra were recorded along the titration (Figure 1D). Upon the addition of FtsZ, we found a couple of residues of MapZ-N undergo significant perturbations in a stepwise directional manner (Figure 1E). In detail, residues including Asn^{7}, Arg^{8}, Gln^{14}, Val^{38}, Val^{76}, Val^{92}, Ser^{95}, Leu^{126}, Glu^{137} possess a chemical shift change above average. To prove whether these residues are indeed involved in the interactions with FtsZ, we constructed a nine-residue mutant of MapZ-N (N7A, R8A, Q14A, V38E, V76E, V92D, S95D, L126D, E137A, termed MapZ-N$_{mut}$) with hydrophilic residues mutated to alanine and hydrophobic residues mutated to aspartate or glutamate. Then we applied MST experiments to quantitatively measure the dissociation constant of MapZ-N$_{mut}$ towards FtsZ. The results gave a K_d of 14.8 ± 5.1 μM (Figure 1F), indicating a much lower binding affinity of MapZ-N$_{mut}$ towards FtsZ, as compared with that of wild-type. Altogether, using a method of much higher resolution, we assigned that a couple of C-terminal residues (V76, V92, S95, L126 and E137) of MapZ-N also contribute to the interaction with FtsZ, in addition to the previously identified residues [31].

MapZ-N facilitates the polymerization of FtsZ to accelerate the activation of GTPase

The direct interactions between MapZ-N and FtsZ indicated that MapZ-N might affect the polymerization and GTPase activity of FtsZ. Thus, we determined the enzymatic parameters of FtsZ in the presence or absence of MapZ-N. We monitored the accumulation of GDP using HPLC after adding GTP at various concentrations ranging from 0.05 to 3 mM. The velocities of GDP production were plotted against the concentrations of input GTP, which could be fitted to the Michaelis–Menten kinetic model. Calculations of enzymatic parameters gave a K_m of 208 ± 32 μM and a V_{max} of 8.97 ± 0.69 μM GTP/μM FtsZ/min (Figure 2A). In contrast, the addition of MapZ-N resulted in a slightly decreased K_m of 167 ± 38 μM and similar V_{max} of 9.32 ± 0.8 μM GTP/μM FtsZ/min (Figure 2B). Despite that the binding of MapZ-N did not significantly alter the catalytic efficiency of FtsZ, a higher Hill coefficient (n_H = 1.71 ± 0.21) of FtsZ in the presence of MapZ-N, compared with without

Biochemical Journal (2019) **476** 1433–1444
https://doi.org/10.1042/BCJ20190138

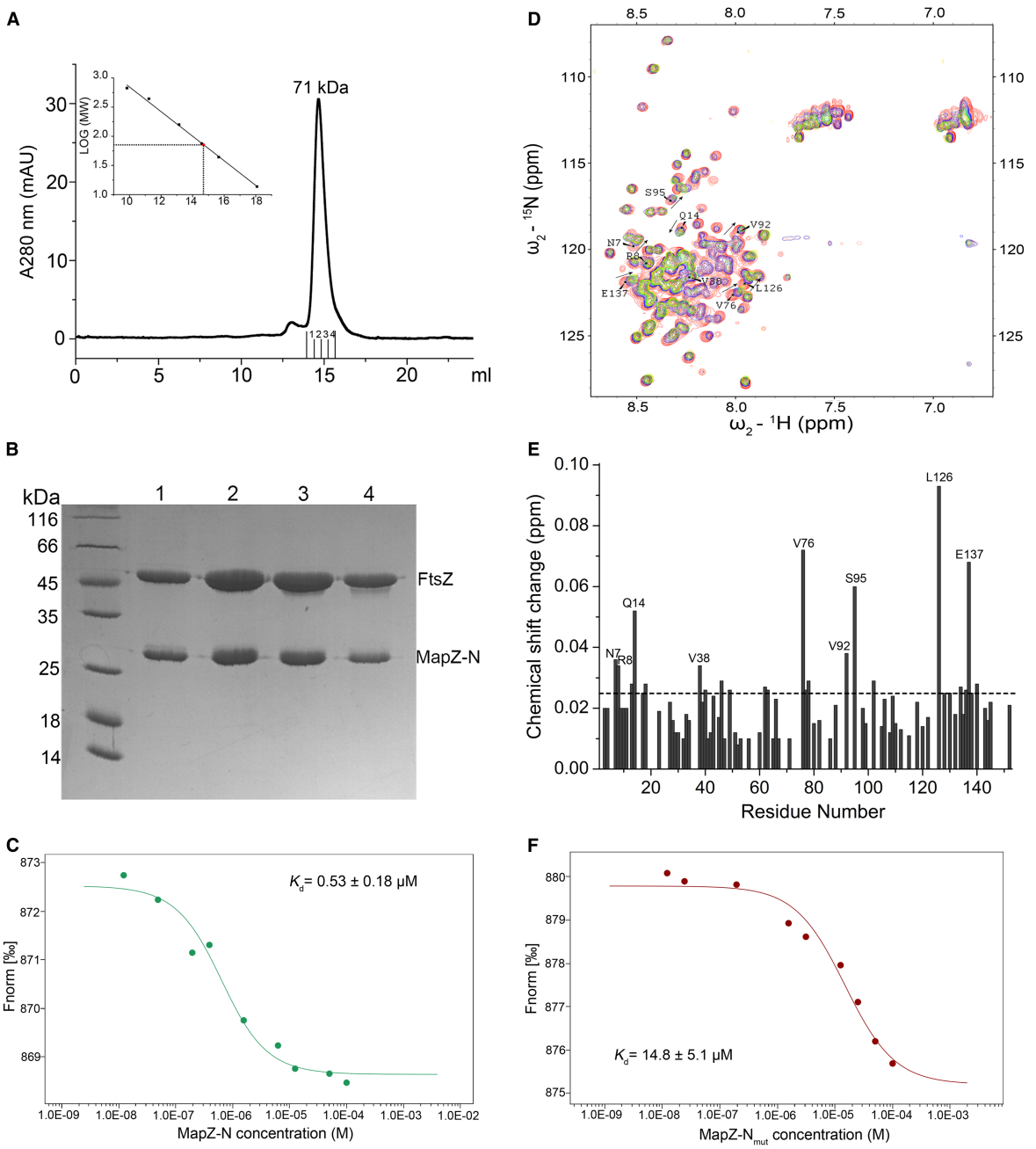

Figure 1. Mapping the key residues of MapZ-N interacting with FtsZ.

(**A**) Gel filtration chromatography of the co-purified MapZ-N and FtsZ. *mAU*, milli-absorbance units. (**B**) Coomassie blue-stained SDS gel electrophoresis of corresponding peak fractions from gel filtration chromatography. The binding affinity of MapZ-N (**C**) and MapZ-N$_{mut}$ (**F**) towards FtsZ determined by MST. (**D**) The ^{1}H–^{15}N HSQC spectra showing significant chemical shift perturbations, which reflect the putative interface residues. (**E**) The histogram plot of the chemical shift changes of MapZ-N induced by addition of FtsZ. The horizontal dashed line denotes the mean value of the chemical shift change. The nine representative residues with a significant chemical shift are labeled.

the addition of MapZ-N ($n_H = 1.35 \pm 0.06$), strongly indicated that the FtsZ molecules catalyze GTP in a much more cooperative manner in the presence of MapZ-N.

Polymerization of FtsZ above a critical protein concentration is essential for the GTPase activity [38]. In fact, we found that hydrolysis of GTP could be detected once the concentration of FtsZ reached 3 μM (Figure 2C).

Biochemical Journal (2019) **476** 1433–1444
https://doi.org/10.1042/BCJ20190138

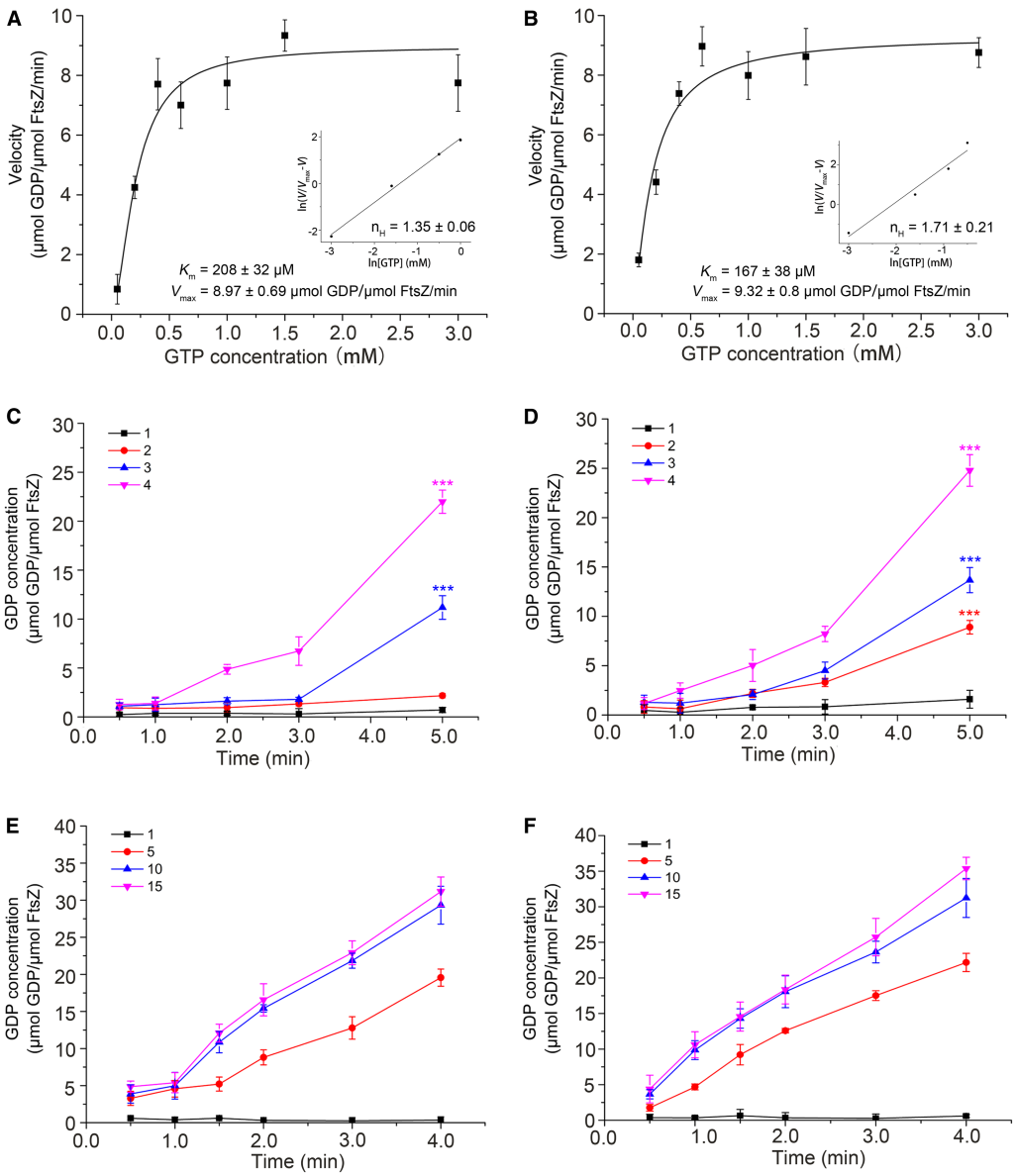

Figure 2. MapZ-N facilitates the polymerization and gain of GTPase activity of FtsZ.

GTP at various concentrations was incubated with 10 μM FtsZ in polymerization buffer in the (**A**) absence or (**B**) presence of MapZ-N. Velocities were obtained from the slopes of the GDP accumulation curves and fitted to the Michaelis–Menten model with a V_{max} of 8.97 ± 0.69 and 9.32 ± 0.8 μmol GTP/μmol FtsZ/min, and a K_m of 208 ± 32 and 167 ± 38 μM, respectively. The Hill plots were shown as insets in Figure 2A,B based on the Hill equation. The critical concentration of FtsZ polymerization is decreased from (**C**) 3 μM in the absence of MapZ-N to (**D**) 2 μM in the presence of MapZ-N at an equal molar ratio. GDP accumulation curves along the time course catalyzed by polymerized FtsZ in the (**E**) absence or (**F**) presence of MapZ-N at an equal molar ratio. The plots were determined at various protein concentrations (squares, 1 μM; circles, 5 μM; up triangles, 10 μM; inverted triangles, 15 μM). Data are presented as the means ± S.D. from three independent assays. Statistical significance analyses were performed using a one-way ANOVA. *** indicates a *P*-value of <0.001.

Given a higher cooperativity of FtsZ in the presence of MapZ, the critical concentration of FtsZ should be reduced. As expected, the results show that critical concentration of FtsZ reduced from 3 to 2 μM in the presence of MapZ-N at an equal molar ratio (Figure 2C,D). Different from other species, *S. pneumoniae* FtsZ assembles through a cooperative mechanism that shows an activation delay of GTP hydrolysis as reported

previously [30]. To further explore whether MapZ-N affects the FtsZ activation delay *in vitro*, we analyzed the enzymatic properties of FtsZ. In agreement with previous results [30], FtsZ showed a delay of GTP hydrolytic activity, which strongly depends on protein concentration, being shorter as FtsZ concentration increased. At 5 μM FtsZ, the delay time is ∼1.5 min, whereas it is shortened to ∼1 min at 10 or 15 μM FtsZ (Figure 2E). The addition of MapZ-N at an equal molar ratio significantly reduces the activation delay time, at 0.5 min for all three concentrations of FtsZ (Figure 2F).

MapZ-N attenuates the bundling of FtsZ oligomers

It was reported that above the critical concentration, the delay of GTPase activity is coupled with the progressive elongation of the FtsZ polymer [30]. As MapZ-N reduces the GTPase activity delay of FtsZ, we next monitored the polymerization/bundling of FtsZ using the 90° light scattering which had been used as a standard method to measure the enhanced signals along the polymerization of FtsZ [28,37]. The polymerization of FtsZ was triggered with GTP and was monitored by light scattering. In the absence of MapZ-N, the polymer is formed in an accelerating manner in the first 3 min and reaches a plateau with the maximum level of polymerization, indicating an equilibrium state of bundling and dissociation (Figure 3A, control). Subsequently, the highly bundled polymers disassembled due to the hydrolysis of GTP driven by the polymerized FtsZ. Upon the addition of MapZ-N, the signal of FtsZ polymerization increases in a much lower velocity and can reach a lower plateau, corresponding to smaller FtsZ bundles. Moreover, the FtsZ polymerization velocity is decreased in a MapZ-N concentration-dependent manner (Figure 3A,B). Addition of MapZ-N leads to less than half of the yield of FtsZ bundled polymers at an equal molar ratio and complete inhibition of polymerization at a MapZ-N concentration of 60 μM. In contrast, the addition of nine-residue mutant MapZ-N (MapZ-N_{mut}) has much less effect on the FtsZ polymerization velocity (Figure 3C,D), indicating this effect is due to direct interactions between FtsZ and MapZ. Notably, deletion of the most C-terminal 12 residues of FtsZ results in a much lower bundling level of FtsZ (Figure 3E,F), further confirming the previous report that FtsZ molecules are bundled via lateral interactions mediated by the C-terminal tail [28]. Moreover, the bundling of FtsZ C-terminal truncated mutant is independent of the presence of MapZ-N, suggesting that MapZ-N inhibits the C-terminal tail mediated filament bundling via competitively interacting with the FtsZ core domain that interacts with the C-terminal tail of the adjacent FtsZ molecule in the same bundle.

To visualize the bundling of FtsZ in solution and the influence of MapZ-N, we applied the negative-staining EM to detect the bundling of FtsZ. As expected, FtsZ proteins at 15 μM exhibit extensive interactions with each other, forming relatively homogenous bundled polymers (Figure 4A). In detail, the bundles share a length of 200–300 nm and a diameter of 12–15 nm, corresponding to ∼3∼4 laterally twisted filaments. Remarkably, some of the FtsZ bundles assemble into a curved structure which mimics the contractive ring for cell division [17], similar to the FtsZ bundling found in *E. coli* [39,40] and *M. tuberculosis* [41]. Upon the addition of 15 μM wild-type MapZ-N, most FtsZ proteins form the single-stranded filaments rather than bundled polymers (Figure 4B). Notably, the addition of the mutant MapZ-N revealed a mix of bundled polymers and single-stranded filaments (Figure 4C). Taken together, we conclude that MapZ-N alters the polymerization process of FtsZ, most likely via lateral interactions with the FtsZ filaments.

Discussion

Streptococcus pneumoniae MapZ was first identified as a scaffold protein that localizes at future division sites before FtsZ and positions the Z-ring correctly via protein–protein interaction [31,32]. Further study suggested that MapZ is important for setting the correct angle of division plane [35]. In addition, structural analysis of the extracellular domain of MapZ suggests that MapZ binds to the peptidoglycan [36] under the control of the Ser/Thr kinase StkP [31], which is a key player in tuning the synthesis of peripheral and septal peptidoglycan [42,43]. However, little is known on the role of the intracellular domain of MapZ during cell division.

Similar to the previous report [30], we confirmed that *S. pneumoniae* FtsZ undergoes an activation delay of GTPase activity, coupling a transition from the inactive monomer to the active polymer form. However, upon binding to the intracellular domain of MapZ, the activation delay is significantly reduced, resulting in a behavior similar to *E. coli* FtsZ, which shows almost no activation delay [30]. It suggested that the presence of MapZ might lower the energy barrier of FtsZ polymerization, which was proved by the lower critical concentration for FtsZ forming a polymer and a higher Hill coefficient towards GTP. Thus, we propose that the intracellular domain of MapZ could facilitate the initiation of FtsZ polymerization.

Biochemical Journal (2019) **476** 1433–1444
https://doi.org/10.1042/BCJ20190138

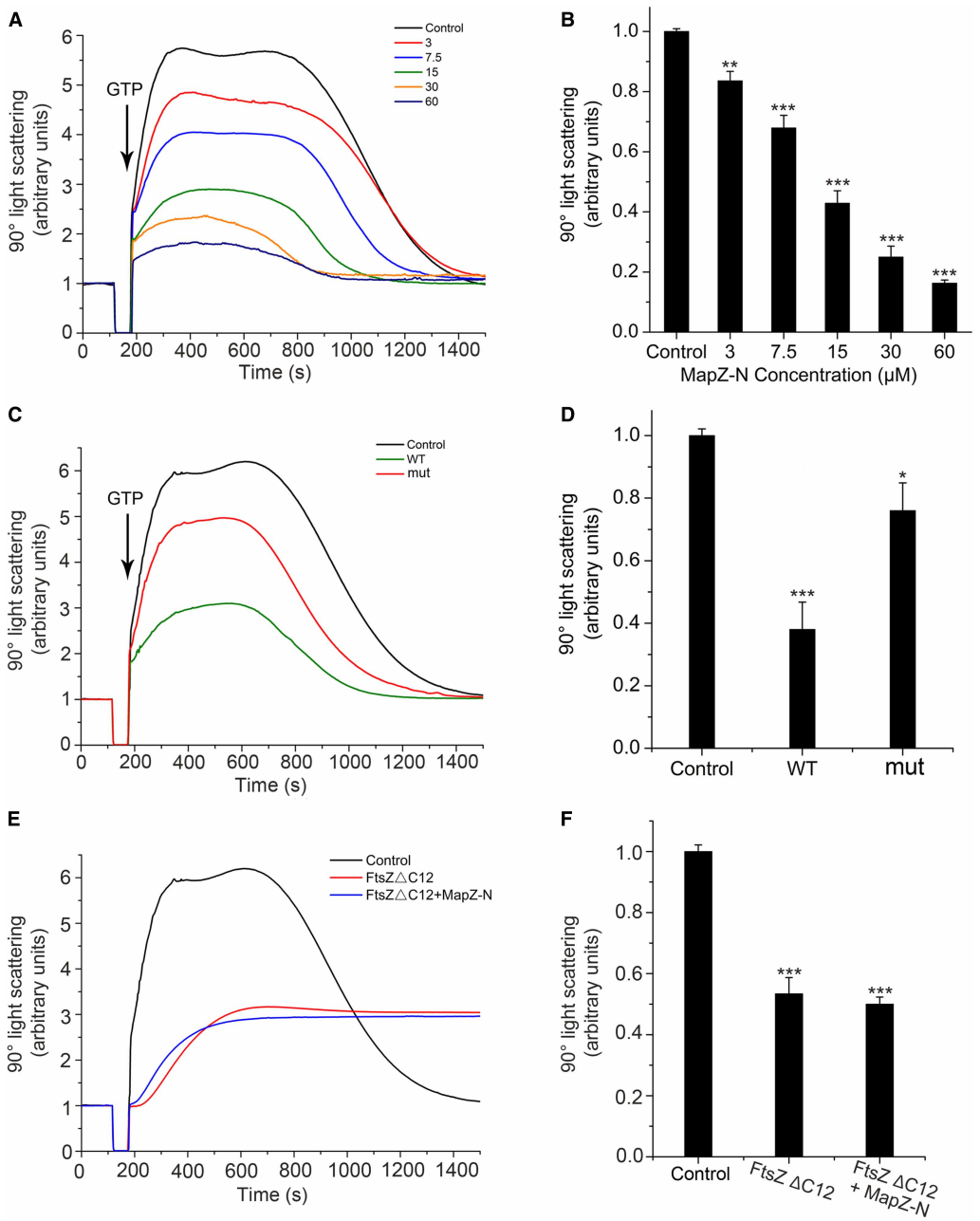

Figure 3. Antagonization of FtsZ bundling by MapZ-N monitored by lights scattering.

The GTP-induced assembly of (**A**) FtsZ in the presence of MapZ-N at various concentrations (3, 7.5, 15, 30, 60 μM) and (**B**) normalized diagram of relative light scattering. (**C**) Comparison of light scattering changed by the addition of wild-type and mutant MapZ-N at an equal molar ratio of FtsZ and (**D**) the normalized diagram. (**E**) MapZ-N inhibits C-terminal tail mediated bundling of FtsZ filaments and (**F**) the normalized diagram. The normalized diagrams were used to compare the maximum light scattering signal in a more illustrative way, using the signal of the control normalized to 1. All versions of FtsZ (WT & FtsZΔC12) used in assays were 15 μM. The arrow indicates the time when GTP was added to a final concentration of 1 mM after baseline recording for 2 min. The arrow corresponds to the time when GTP was added to a final concentration of 1 mM after baseline recording in 2 min. The results shown are the mean ± S.D. from three independent measurements. Statistical significance analyses were performed using a one-way ANOVA. *P*-value of <0.05, 0.01 and 0.001 are indicated with *, ** and ***, respectively.

Biochemical Journal (2019) **476** 1433–1444
https://doi.org/10.1042/BCJ20190138

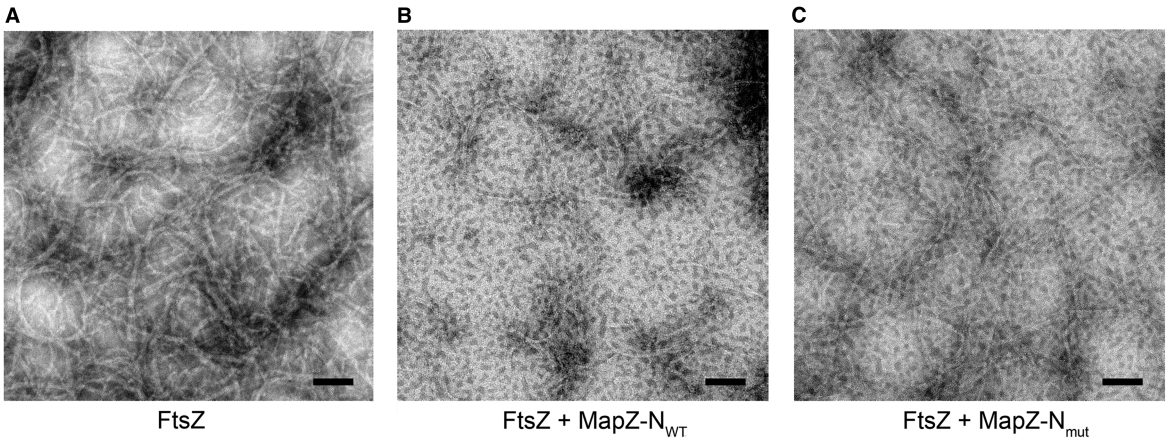

Figure 4. Electron microscopic pictures of FtsZ polymers.

Negative stain electron micrographs of FtsZ at 15 μM in the (**A**) absence or presence of equal molar ratio of (**B**) MapZ-N or (**C**) MapZ-N$_{mut}$. All samples were prepared for electron microscopy as described in the Materials and Methods. The scale bar is 100 nm.

It has long been recognized that the *in vivo* FtsZ forms a compact closed ring-like structure [44–47]. However, accumulating evidences showed that Z-ring is composed of a loose bundle of FtsZ filaments that randomly overlap with each other, especially at the onset of bacteria cytokinesis [7,13–17]. The bundling of Z-ring with favorable lateral interactions between FtsZ filaments may serve as a navigator to recruit the cell wall synthesis machinery, which contributes to the main constriction force of cell separation [7,48]. Thus, it is important to maintain dynamic and loosely bundled FtsZ filaments to provide a proper timing and enough space for the recruitment of other cell division proteins into the divisome. To coordinate the precise cell division process, several regulators have been identified that act in concert to regulate FtsZ polymerization via distinct mechanisms, such as ZapA-E in *E. coli* and SepF, EzrA in *B. subtilis* and *S. pneumoniae* [27,49,50]. In addition to these Z-ring structure regulators, it is reported that C-terminal tail of FtsZ itself also determines the lateral interaction pattern [28]. Here we further confirmed that the C-terminal tail is indispensable for the bundling of FtsZ (Figure 3E,F). However, the process and final structure of FtsZ bundles should be finely controlled, in the present case, via the lateral interactions with MapZ. On the other hand, the released C-terminal tail is ready to recruit other cell division proteins, such as FtsA, EzrA and SepF in *S. pneumoniae*.

Altogether, these findings enabled us to propose a model for MapZ-coordinated FtsZ structure and dynamics in *S. pneumoniae* (Figure 5). At the initial state of cell division, MapZ are aligned at the division site

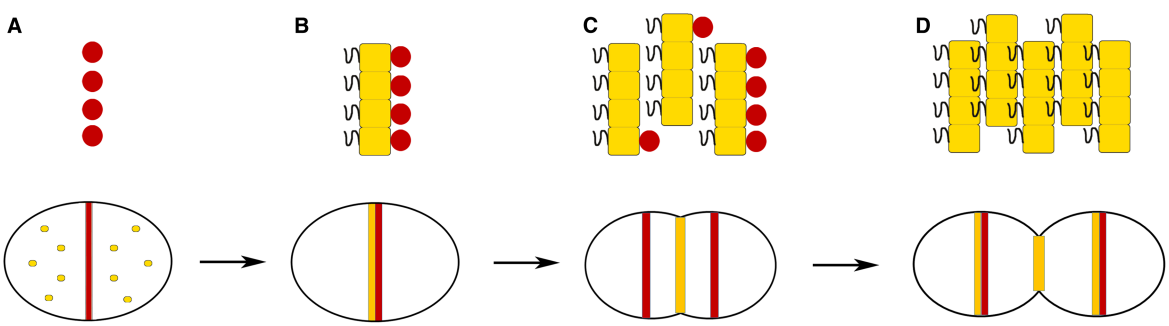

Figure 5. A proposed model for the multiple functions of MapZ.

The upper panel of the figure highlights the two proteins MapZ and FtsZ at different states. (**A**) MapZ molecules aligned along the future septum. (**B**) FtsZ monomers recruited by MapZ forming single-stranded filaments with MapZ laterally binding to the core domain. (**C**) Loosely bundled FtsZ polymers. (**D**) Condensed bundle of FtsZ in the Z-ring. MapZ is shown as a red dot, whereas FtsZ is shown as a yellow rectangle with a black tail.

Biochemical Journal (2019) **476** 1433–1444
https://doi.org/10.1042/BCJ20190138

(Figure 5A), via its extracellular domain that recognizes the nascent peptidoglycan [31]. Subsequently, the intracellular domain of MapZ starts to recruit FtsZ monomers and triggers the polymerization of FtsZ into single-stranded filaments (Figure 5B). The lateral interactions with MapZ make FtsZ form loosely bundled polymers (Figure 5C), which might facilitate the recruitment of other cell division proteins via its C-terminal tails. In turn, the MapZ molecules are moved away from the septum along with the synthesis of peptidoglycan and aligned at the next-cycle division site. As the mother cell elongates, the FtsZ ring condenses (Figure 5D) to navigate cell wall synthesis machinery until the production of two daughter cells.

Distinct from the previously identified regulators, which are either positive [51,52] or negative [51] towards the assembly of FtsZ, *S. pneumoniae* MapZ is a double-edged sword for FtsZ. On one hand, at the very beginning of cell division, MapZ acts as a master regulator that controls the precise positioning of FtsZ and a trigger that facilitates the formation of FtsZ single-stranded filaments. On the other hand, the lateral interactions with FtsZ core domain enabled the formation and maintenance of loosely bundled polymer of FtsZ, which is important for the dynamic and proper timing for cell division. In sum, MapZ is a multi-functional regulator that controls both the precise positioning and timing of FtsZ polymerization.

Database depositions

The NMR chemical shift data have been deposited in the Biological Magnetic Data Bank with accession number 27608.

Abbreviations

FtsZ, filamentous temperature-sensitive Z; GTP, guanosine-5'-triphosphate; HSQC, heteronuclear single quantum coherence; IPTG, isopropyl β-D-1-thiogalactopyranoside; MapZ, mid-cell-anchored protein Z; MapZ-N, the intracellular domain of MapZ; MapZ-N_{mut}, the 9-residue mutant of MapZ-N; MST, microscale thermophoresis; NMR, nuclear magnetic resonance; Z-ring, a ring-like structure polymerized by FtsZ at mid-cell.

Author Contribution

Z.F., Y.-L.J., Y.C. and C.-Z.Z. designed the study, analyzed the data and wrote the paper. Z.F. and D.X. performed the biochemical and enzymatic experiments; J.H.Z. performed NMR spectroscopy and processed the data.

Funding

This work is supported by the National Natural Science Foundation of China [http://www.nsfc.gov.cn, Grant No. 31670732, 31770787 and 31621002], and the Ministry of Science and Technology of China [http://www.most.gov.cn, Grants No. 2016YFA0400900].

Acknowledgements

We thank the staff at the Core Facility Center for Life Sciences at University of Science and Technology of China for technical assistance.

Competing Interests

The Authors declare that there are no competing interests associated with the manuscript.

References

1 Bi, E.F. and Lutkenhaus, J. (1991) Ftsz ring structure associated with division in *Escherichia coli*. *Nature* **354**, 161–164 https://doi.org/10.1038/354161a0
2 Adams, D.W. and Errington, J. (2009) Bacterial cell division: assembly, maintenance and disassembly of the Z ring. *Nat. Rev. Microbiol.* **7**, 642–653 https://doi.org/10.1038/nrmicro2198
3 Natale, P., Pazos, M. and Vicente, M. (2013) The *Escherichia coli* divisome: born to divide. *Environ. Microbiol.* **15**, 3169–3182 https://doi.org/10.1111/1462-2920.12227
4 Lutkenhaus, J., Pichoff, S. and Du, S.S. (2012) Bacterial cytokinesis: from Z ring to divisome. *Cytoskeleton* **69**, 778–790 https://doi.org/10.1002/cm.21054
5 Egan, A.J.F. and Vollmer, W. (2013) The physiology of bacterial cell division. *Ann. N. Y. Acad. Sci.* **1277**, 8–28 https://doi.org/10.1111/j.1749-6632.2012.06818.x
6 Haeusser, D.P. and Margolin, W. (2016) Splitsville: structural and functional insights into the dynamic bacterial Z ring. *Nat. Rev. Microbiol.* **14**, 205–319 https://doi.org/10.1038/nrmicro.2016.7

7 Coltharp, C., Buss, J., Plumer, T.M. and Xiao, J. (2016) Defining the rate-limiting processes of bacterial cytokinesis. *Proc. Natl Acad. Sci. U.S.A.* **113**, E1044–E1053 https://doi.org/10.1073/pnas.1514296113
8 Coltharp, C. and Xiao, J. (2017) Beyond force generation: why is a dynamic ring of FtsZ polymers essential for bacterial cytokinesis? *Bioessays* **39**, 1–11 https://doi.org/10.1002/bies.201600179
9 Stricker, J., Maddox, P., Salmon, E.D. and Erickson, H.P. (2002) Rapid assembly dynamics of the *Escherichia coli* FtsZ-ring demonstrated by fluorescence recovery after photobleaching. *Proc. Natl Acad. Sci. U.S.A.* **99**, 3171–3175 https://doi.org/10.1073/pnas.052595099
10 Rueda, S., Vicente, M. and Mingorance, J. (2003) Concentration and assembly of the division ring proteins FtsZ, FtsA, and ZipA during the *Escherichia coli* cell cycle. *J. Bacteriol.* **185**, 3344–3351 https://doi.org/10.1128/JB.185.11.3344-3351.2003
11 Pogliano, J., Pogliano, K., Weiss, D.S., Losick, R. and Beckwith, J. (1997) Inactivation of FtsI inhibits constriction of the FtsZ cytokinetic ring and delays the assembly of FtsZ rings at potential division sites. *Proc. Natl Acad. Sci. U.S.A.* **94**, 559–564 https://doi.org/10.1073/pnas.94.2.559
12 Sun, Q. and Margolin, W. (1998) Ftsz dynamics during the division cycle of live *Escherichia coli* cells. *J. Bacteriol.* **180**, 2050–2056 PMID:9555885
13 Strauss, M.P., Liew, A.T., Turnbull, L., Whitchurch, C.B., Monahan, L.G. and Harry, E.J. (2012) 3D-SIM super resolution microscopy reveals a bead-like arrangement for FtsZ and the division machinery: implications for triggering cytokinesis. *PLoS Biol.* **10**, e1001389 https://doi.org/10.1371/journal.pbio.1001389
14 Holden, S.J., Pengo, T., Meibom, K.L., Fernandez Fernandez, C., Collier, J. and Manley, S. (2014) High throughput 3D super-resolution microscopy reveals *Caulobacter crescentus* in vivo Z-ring organization. *Proc. Natl Acad. Sci. U.S.A.* **111**, 4566–4571 https://doi.org/10.1073/pnas.1313368111
15 Fu, G., Huang, T., Buss, J., Coltharp, C., Hensel, Z. and Xiao, J. (2011) In vivo structure of the *E. coli* FtsZ-ring revealed by photoactivated localization microscopy (PALM). *Biophys. J.* **100**, 615–615 https://doi.org/10.1016/j.bpj.2010.12.3542
16 Jacq, M., Adam, V., Bourgeois, D., Moriscot, C., Di Guilmi, A.M., Vernet, T. et al. (2015) Remodeling of the Z-ring nanostructure during the *Streptococcus pneumoniae* cell cycle revealed by photoactivated localization microscopy. *mBio* **6**, e01108–e01115 https://doi.org/10.1128/mBio.01108-15
17 Li, Z., Trimble, M.J., Brun, Y.V. and Jensen, G.J. (2007) The structure of FtsZ filaments in vivo suggests a force-generating role in cell division. *EMBO J.* **26**, 4694–4708 https://doi.org/10.1038/sj.emboj.7601895
18 Rivas, G., López, A., Mingorance, J., Ferrándiz, M.J., Zorrilla, S., Minton, A.P. et al. (2000) Magnesium-induced linear self-association of the FtsZ bacterial cell division protein monomer – the primary steps for FtsZ assembly. *J. Biol. Chem.* **275**, 11740–11749 https://doi.org/10.1074/jbc.275.16.11740
19 Romberg, L., Simon, M. and Erickson, H.P. (2001) Polymerization of FtsZ, a bacterial homolog of tubulin. Is assembly cooperative? *J. Biol. Chem.* **276**, 11743–11753 https://doi.org/10.1074/jbc.M009033200
20 Caplan, M.R. and Erickson, H.P. (2003) Apparent cooperative assembly of the bacterial cell division protein FtsZ demonstrated by isothermal titration calorimetry. *J. Biol. Chem.* **278**, 13784–13788 https://doi.org/10.1074/jbc.M300860200
21 González, J.M., Jiménez, M., Vélez, M., Mingorance, J., Andreu, J.M., Vicente, M. et al. (2003) Essential cell division protein FtsZ assembles into one monomer-thick ribbons under conditions resembling the crowded intracellular environment. *J. Biol. Chem.* **278**, 37664–37671 https://doi.org/10.1074/jbc.M305230200
22 Romberg, L. and Mitchison, T.J. (2004) Rate-limiting guanosine 5′-triphosphate hydrolysis during nucleotide turnover by FtsZ, a prokaryotic tubulin homologue involved in bacterial cell division. *Biochemistry* **43**, 282–288 https://doi.org/10.1021/bi035465r
23 Chen, Y.D., Bjornson, K., Redick, S.D. and Erickson, H.P. (2005) A rapid fluorescence assay for FtsZ assembly indicates cooperative assembly with a dimer nucleus. *Biophys. J.* **88**, 505–514 https://doi.org/10.1529/biophysj.104.044149
24 Milam, S.L. and Erickson, H.P. (2013) Rapid in vitro assembly of *Caulobacter crescentus* FtsZ protein at pH 6.5 and 7.2. *J. Biol. Chem.* **288**, 23675–23679 https://doi.org/10.1074/jbc.M113.491845
25 Erickson, H.P., Anderson, D.E. and Osawa, M. (2010) Ftsz in bacterial cytokinesis: cytoskeleton and force generator all in one. *Microbiol. Mol. Biol. Rev.* **74**, 504–528 https://doi.org/10.1128/MMBR.00021-10
26 Szwedziak, P., Wang, Q., Bharat, T.A.M., Tsim, M. and Löwe, J. (2014) Architecture of the ring formed by the tubulin homologue FtsZ in bacterial cell division. *eLife* **3**, e04601 https://doi.org/10.7554/eLife.04601
27 Ortiz, C., Natale, P., Cueto, L. and Vicente, M. (2016) The keepers of the ring: regulators of FtsZ assembly. *FEMS Microbiol. Rev.* **40**, 57–67 https://doi.org/10.1093/femsre/fuv040
28 Buske, P.J. and Levin, P.A. (2012) Extreme C terminus of bacterial cytoskeletal protein FtsZ plays fundamental role in assembly independent of modulatory proteins. *J. Biol. Chem.* **287**, 10945–10957 https://doi.org/10.1074/jbc.M111.330324
29 Huang, K.H., Mychack, A., Tchorzewski, L. and Janakiraman, A. (2016) Characterization of the FtsZ C-terminal variable (CTV) region in Z-ring assembly and interaction with the Z-ring stabilizer ZapD in *E. coli* cytokinesis. *PLoS ONE* **11**, e0153337 https://doi.org/10.1371/journal.pone.0153337
30 Salvarelli, E., Krupka, M., Rivas, G., Mingorance, J., Gómez-Puertas, P., Alfonso, C. et al. (2015) The cell division protein FtsZ from *Streptococcus pneumoniae* exhibits a GTPase activity delay. *J. Biol. Chem.* **290**, 25081–25089 https://doi.org/10.1074/jbc.M115.650077
31 Fleurie, A., Lesterlin, C., Manuse, S., Zhao, C., Cluzel, C., Lavergne, J.P. et al. (2014) Mapz marks the division sites and positions FtsZ rings in *Streptococcus pneumoniae*. *Nature* **516**, 259–262 https://doi.org/10.1038/nature13966
32 Holečková, N., Doubravová, L., Massidda, O., Molle, V., Buriánková, K., Benada, O. et al. (2015) Locz is a new cell division protein involved in proper septum placement in *Streptococcus pneumoniae*. *mBio* **6**, e01700–e01714 https://doi.org/10.1128/mBio.01700-14
33 Barák, I. and Wilkinson, A.J. (2007) Division site recognition in *Escherichia coli* and *Bacillus subtilis*. *FEMS Microbiol. Rev.* **31**, 311–326 https://doi.org/10.1111/j.1574-6976.2007.00067.x
34 Monahan, L.G., Liew, A.T., Bottomley, A.L. and Harry, E.J. (2014) Division site positioning in bacteria: one size does not fit all. *Front. Microbiol.* **5**, 19 https://doi.org/10.3389/fmicb.2014.00019
35 van Raaphorst, R., Kjos, M. and Veening, J.W. (2017) Chromosome segregation drives division site selection in *Streptococcus pneumoniae*. *Proc. Natl Acad. Sci. U.S.A.* **114**, E5959–E5968 https://doi.org/10.1073/pnas.1620608114
36 Manuse, S., Jean, N.L., Guinot, M., Lavergne, J.P., Laguri, C., Bougault, C.M. et al. (2016) Structure-function analysis of the extracellular domain of the pneumococcal cell division site positioning protein MapZ. *Nat. Commun.* **7**, 12071 https://doi.org/10.1038/ncomms12071
37 Mukherjee, A. and Lutkenhaus, J. (1999) Analysis of FtsZ assembly by light scattering and determination of the role of divalent metal cations. *J. Bacteriol.* **181**, 823–832 PMID:9922245

Biochemical Journal (2019) **476** 1433–1444
https://doi.org/10.1042/BCJ20190138

38 Lan, G., Dajkovic, A., Wirtz, D. and Sun, S.X. (2008) Polymerization and bundling kinetics of FtsZ filaments. *Biophys. J.* **95**, 4045–4056 https://doi.org/10.1529/biophysj.108.132837
39 Lu, C.L., Reedy, M. and Erickson, H.P. (2000) Straight and curved conformations of FtsZ are regulated by GTP hydrolysis. *J. Bacteriol.* **182**, 164–170 https://doi.org/10.1128/JB.182.1.164-170.2000
40 Pacheco-Gómez, R., Roper, D.I., Dafforn, T.R. and Rodger, A. (2011) The pH dependence of polymerization and bundling by the essential bacterial cytoskeletal protein FtsZ. *PLoS ONE* **6**, e19369 https://doi.org/10.1371/journal.pone.0019369
41 Chen, Y., Anderson, D.E., Rajagopalan, M. and Erickson, H.P. (2007) Assembly dynamics of *Mycobacterium tuberculosis* FtsZ. *J. Biol. Chem.* **282**, 27736–27743 https://doi.org/10.1074/jbc.M703788200
42 Beilharz, K., Novakova, L., Fadda, D., Branny, P., Massidda, O. and Veening, J.W. (2012) Control of cell division in *Streptococcus pneumoniae* by the conserved Ser/Thr protein kinase StkP. *Proc. Natl Acad. Sci. U.S.A.* **109**, E905–E913 https://doi.org/10.1073/pnas.1119172109
43 Fleurie, A., Manuse, S., Zhao, C., Campo, N., Cluzel, C., Lavergne, J.P. et al. (2014) Interplay of the serine/threonine-kinase StkP and the paralogs DivIVA and GpsB in pneumococcal cell elongation and division. *PLoS Genet* **10**, e1004275 https://doi.org/10.1371/journal.pgen.1004275
44 Ben-Yehuda, S. and Losick, R. (2002) Asymmetric cell division in *B. subtilis* involves a spiral-like intermediate of the cytokinetic protein FtsZ. *Cell* **109**, 257–266 https://doi.org/10.1016/S0092-8674(02)00698-0
45 Peters, P.C., Migocki, M.D., Thoni, C. and Harry, E.J. (2007) A new assembly pathway for the cytokinetic Z ring from a dynamic helical structure in vegetatively growing cells of *Bacillus subtilis*. *Mol. Microbiol.* **64**, 487–499 https://doi.org/10.1111/j.1365-2958.2007.05673.x
46 Ma, X., Ehrhardt, D.W. and Margolin, W. (1996) Colocalization of cell division proteins FtsZ and FtsA to cytoskeletal structures in living *Escherichia coli* cells by using green fluorescent protein. *Proc. Natl Acad. Sci. U.S.A.* **93**, 12998–13003 https://doi.org/10.1073/pnas.93.23.12998
47 Thanedar, S. and Margolin, W. (2004) Ftsz exhibits rapid movement and oscillation waves in helix-like patterns in *Escherichia coli*. *Curr. Biol.* **14**, 1167–1173 https://doi.org/10.1016/j.cub.2004.06.048
48 Lan, G.H., Daniels, B.R., Dobrowsky, T.M., Wirtz, D. and Sun, S.X. (2009) Condensation of FtsZ filaments can drive bacterial cell division. *Proc. Natl Acad. Sci. U.S.A.* **106**, 121–126 https://doi.org/10.1073/pnas.0807963106
49 Duman, R., Ishikawa, S., Celik, I., Strahl, H., Ogasawara, N., Troc, P. et al. (2013) Structural and genetic analyses reveal the protein SepF as a new membrane anchor for the Z ring. *Proc. Natl Acad. Sci. U.S.A.* **110**, E4601–E4610 https://doi.org/10.1073/pnas.1313978110
50 Cleverley, R.M., Barrett, J.R., Baslé, A., Bui, N.K., Hewitt, L., Solovyova, A. et al. (2014) Structure and function of a spectrin-like regulator of bacterial cytokinesis. *Nat. Commun.* **5**, 5421 https://doi.org/10.1038/ncomms6421
51 Willemse, J., Borst, J.W., de Waal, E., Bisseling, T. and van Wezel, G.P. (2011) Positive control of cell division: FtsZ is recruited by SsgB during sporulation of *Streptomyces*. *Gene Dev* **25**, 89–99 https://doi.org/10.1101/gad.600211
52 Treuner-Lange, A., Aguiluz, K., van der Does, C., Gómez-Santos, N., Harms, A., Schumacher, D. et al. (2013) Pomz, a ParA-like protein, regulates Z-ring formation and cell division in *Myxococcus xanthus*. *Mol. Microbiol.* **87**, 235–253 https://doi.org/10.1111/mmi.12094